Inorg. Chem. **2007**, *46*, 3839–3850

Structure and Bonding in $SnWO_4$, $PbWO_4$, and $BiVO_4$: Lone Pairs vs Inert Pairs

Matthew W. Stoltzfus, Patrick M. Woodward,* Ram Seshadri,[†] Jae-Hyun Klepeis,[‡] and Bruce Bursten[§]

Department of Chemistry, Ohio State University, 100 West 18th Avenue, Columbus, Ohio 43210, Materials Department, University of California, Santa Barbara, California 93106, Lawrence Livermore National Laboratory, Livermore, California 94550, and Department of Chemistry, The University of Tennessee, Knoxville, Tennessee 37996

Received June 25, 2006

Three ternary oxides, $SnWO_4$, $PbWO_4$, and $BiVO_4$, containing p-block cations with ns^2np^0 electron configurations, so-called lone pair cations, have been studied theoretically using density functional theory and UV–visible diffuse reflectance spectroscopy. The computations reveal significant differences in the underlying electronic structures that are responsible for the varied crystal chemistry of the lone pair cations. The filled 5s orbitals of the Sn^{2+} ion interact strongly with the 2p orbitals of oxygen, which leads to a significant destabilization of symmetric structures (scheelite and zircon) favored by electrostatic forces. The destabilizing effect of this interaction can be significantly reduced by lowering the symmetry of the Sn^{2+} site to enable the antibonding Sn 5s–O 2p states to mix with the unfilled Sn 5p orbitals. This interaction produces a localized, nonbonding state at the top of the valence band that corresponds closely with the classical notion of a stereoactive electron lone pair. In compounds containing Pb^{2+} and Bi^{3+} the relativistic contraction of the 6s orbital reduces its interaction with oxygen, effectively diminishing its role in shaping the crystal chemical preferences of these ions. In $PbWO_4$ this leads to a stabilization of the symmetric scheelite structure. In the case of $BiVO_4$ the energy of the Bi 6s orbital is further stabilized. Despite this stabilization, the driving force for a stereoactive lone pair distortion appears to be enhanced. The energies of structures exhibiting distorted Bi^{3+} environments are competitive with structures that possess symmetric Bi^{3+} environments. Nevertheless, the "lone pair" that results associated with a distorted Bi^{3+} environment in $BiVO_4$ is more diffuse than the Sn^{2+} lone pair in β-$SnWO_4$. Furthermore, the distortion has a much smaller impact on the electronic structure near the Fermi level.

Introduction

The presence of a filled cation s-subshell has a pronounced impact on the crystal chemistry of p-block cations with ns^2np^0 electron configurations. In particular, the "nonbonding" pair of electrons often becomes stereochemically active. The stereochemically active electron lone pair distortion is traditionally explained by invoking mixing of the cation s and p orbitals to form a nonbonding lobe of electron density that occupies one of the coordination sites surrounding the central cation. The presence of a stereochemically active electron lone pair on the central cation impacts the spatial distribution of the bonding electron pairs, resulting in an asymmetric local environment. In some instances the dipoles associated with the asymmetric local coordination environment are oriented in a manner that gives rise to non-centrosymmetric crystal structures and properties such as ferroelectricity, piezoelectricity, and nonlinear optical behavior.

The role of lone pair distortions in structural chemistry has been addressed many times over the past six decades, in both molecular and solid-state chemistry. Sidgwick–Powell theory (1940) stated that bonding pairs and lone pairs are of equal importance and these pairs distribute themselves so as to minimize electrostatic repulsive interactions. However, this theory did not account for some of the more quantitative aspects of molecular geometry, such as deviations of the bond angles in H_2O and NH_3 from the 109.5° value expected for a symmetric tetrahedron.[1] Gillespie and Nyholm proposed the valence shell electron pair repulsion

* To whom correspondence should be addressed. E-mail: woodward@chemistry.ohio-state.edu. Fax: 1-614-292-1362.
[†] University of California.
[‡] Lawrence Livermore National Laboratory.
[§] The University of Tennessee.

10.1021/ic061157g CCC: $37.00
Published on Web 04/19/2007

(VSEPR) theory in 1957.[2] VSEPR theory explained the bond angles in H_2O and NH_3, as well as the locations of the lone pairs and bonding pairs in ClF_3. In the 1950s Orgel explained lone pair effects by invoking intra-atomic mixing of cation s and cation p orbitals.[3] Two decades later, Andersson and co-workers carried out a number of insightful analyses on the crystal chemistry of cation-based lone pairs in oxides and fluorides.[4,5] The findings of these studies can be summarized as follows. (a) The lone pair possesses approximately the same volume as an oxide or fluoride anion, (b) the lone pair−nucleus distance is significantly shorter than the corresponding anion−cation internuclear separation, and (c) the presence of a lone pair leads to an off-centric displacement of the cation from the centroid of its coordination polyhedron.

In 1984 Bersuker argued that the stereoactivity is determined by the energy separation between the cation-based highest occupied molecular orbital (HOMO) and the anion-based lowest unoccupied molecular orbital (LUMO).[6] In 1999 computational work by Watson and Parker on PbO led them to conclude that lone pair distortions are driven primarily by cation−oxygen interactions.[7,8] Subsequently, Waghmare et al. systematically studied the role of the cation−anion interaction and showed that lone pair formation is driven primarily by the covalent interaction between cation s and anion p states mediated by the cation p states.[9] Walsh and Watson reached a similar conclusion in a computational study of the Sn(II) monochalcogenides (SnO, SnS, SnSe, and SnTe), although they describe the orbital mixing as anion p states mediating the interaction between Sn 5s and 5p states.[10] Mudring and Rieger carried out computational studies of Tl^+ ions in crown ethers and reached the conclusion that antibonding interactions between the Tl 6s orbitals and the oxygens in the crown ether drive the lone pair distortion.[11] These studies have altered the accepted view of lone pair distortions. Orgel's explanation that emphasizes intra-atomic rehybridation of the cation orbitals has been superseded by the notion that cation−anion interactions are the true driving force behind lone pair distortions.

Occupation of the s subshell does not always lead to stereochemical activity. In some cases, such as GeTe, the cation−anion orbital mixing is so extensive that the electrons in the s subshell become delocalized and metallic conductivity results. In other cases, such as PbTe, the coordination environment of the p-block cation remains symmetric and the valence shell s electrons remain highly localized.[9] In the latter case the ns^2 electron pair might be more accurately described as an *inert pair* rather than a *lone pair*. Brown has shown that the local environment of the Tl^+ ion, with $6s^26p^0$ electron configuration, can vary from completely symmetric to highly distorted depending upon the bonding strength of the anion.[12] In more complex compositions a given cation−anion pair may exhibit varying preferences for either *inert pair* or *lone pair* behavior. Consider for example the crystal chemical behavior of the Pb^{2+} ion in oxides. In both polymorphs of PbO the Pb^{2+} ions exhibit a pronounced stereochemical electron lone pair distortion,[13] yet in a number of ternary oxides, including $PbWO_4$, the oxygen forms strong bonds to another cation which in turn leads to a weakening of the bonds to the Pb^{2+} cation thereby stabilizing a symmetric Pb^{2+} environment.[14] Another factor that can influence the stereochemical activity of a given cation−anion pair (or lack thereof) is the topology of the crystal structure, as will be discussed in this paper for the zircon[15] and scheelite[16] polymorphs of $BiVO_4$.

There is also general interest in the horizontal and vertical periodic trends in the stereochemical activity of ns^2np^0 cations. A reduction in the cation s−anion p interaction as a result of relativistic effects is generally accepted to be responsible for the decreased tendency of sixth-period elements to show lone pair distortions.[9−11,17] However, the horizontal trends are not so easy to rationalize. Recent studies of sixth-period post-transition metal binary oxides, involving X-ray spectroscopy and density functional theory computations, show unequivocally that the majority of the 6s electronic states are located below the oxygen 2p valence band.[18−21] Furthermore, the cation 6s−oxygen 2p covalency is shown to steadily decrease upon moving left-to-right from Hg to Bi.[20,21]

Interestingly the stereochemical activity of the lone electron pair seems to increase upon moving from left to right. For example, TlCl adopts the symmetric CsCl structure,[22] $PbCl_2$ adopts a structure with a relatively small lone pair distortion (Pb^{2+} is seven-coordinate with Pb−Cl bond distances ranging from 2.85 to 3.08 Å),[23] and $BiCl_3$ adopts a structure with a very pronounced lone pair distortion (three Bi−Cl bonds in the range 2.45−2.52 Å, three Bi−Cl bonds

(1) Sidgwick, N. V.; Powell, H. M. *Proc. R. Soc. (London)* **1940**, *A176*, 153.
(2) Gillespie, R. J.; Nyholm, R. S. *Quart. Rev. London* **1957**, *11*, 339.
(3) Orgel, L. E. *J. Chem. Soc.* **1959**, *4*, 3815.
(4) Galy, J.; Meunier, G.; Andersson, S.; Astrom, A. *J. Solid State Chem.* **1975**, *13* (1−2), 142.
(5) Andersson, S. *Acta Crystallogr.* **1979**, *B35*, 1321.
(6) Bersuker, I. B. *The Jahn-Teller Effect and Vibronic Interactions in Modern Chemistry*; Plenum: New York, 1984.
(7) Watson, G. W.; Parker, S. C. *J. Phys. Chem. B* **1999**, *103* (8), 1258.
(8) Watson, G. W.; Parker, S. C.; Kresse, G. *Phys. Rev. B* **1999**, *59* (13), 8481.
(9) Waghmare, U. V.; Spaldin, N. A.; Kandpal, H. C.; Seshadri, R. *Phys. Rev. B* **2003**, *67*, 125111.
(10) Walsh, A.; Watson, G. W. *J. Phys. Chem. B* **2005**, *109*, 18868.
(11) Mudring, A. V.; Rieger, F. *Inorg. Chem.* **2005**, *44*, 6240.
(12) Brown, I. D. *The Chemical Bond in Inorganic Chemistry*; IUCr Monographs on Crystallography, Vol. 12; Oxford University Press: New York, 2002.
(13) Leciejewicz, J. *Acta Crystallogr.* **1961**, *14*, 1304. Hill, R. J. *Acta Crystallogr.* **1985**, *C41*, 1281.
(14) Vegard, L.; Refsum, A. *Norske Vid. Akad. Skr. Oslo Math. Nat. Kl.* **1927**, (No. 2).
(15) Dreyer, G.; Tillmanns, E. *Neues Jahrb. Mineral., Monatsh.* **1981**, 151.
(16) Sleight, A. W.; Chen, H. Y.; Ferretti, A.; Cox, D. E. *Mater. Res. Bull.* **1979**, *14*, 1571.
(17) Walsh, A.; Watson, G. W. *J. Solid State Chem.* **2005**, *178*, 1422.
(18) Glans, P. A.; Learmonth, T.; McGuinness, C.; Smith, K. E.; Guo, J.; Walsh, A.; Watson, G. W.; Egdell, R. G. *Chem. Phys. Lett.* **2004**, *399*, 98.
(19) Glans, P. A.; Learmonth, T.; Smith, K. E.; Guo, J.; Walsh, A.; Watson, G. W.; Terzi, F. Egdell, R. G. *Phys. Rev. B* **2005**, *71*, 235109.
(20) Payne, D. J.; Egdell, R. G.; Walsh, A.; Watson, G. W.; Guo, J.; Glans, P. A.; Learmonth, T.; Smith, K. E. *Phys. Rev. Lett.* **2006**, *96*, 157403.
(21) Walsh, A.; Watson, G. W.; Payne, D. J.; Egdell, R.; Guo, J.; Glans, P. A.; Learmonth, T.; Smith, K. E. *Phys. Rev. B* **2006**, *73*, 235104.
(22) Smakula, A.; Kalnajs, J. *Phys. Rev.* **1955**, *99*, 1737.
(23) Nozik, Yu. Z.; Fykin, L. E.; Muradyan, L. A. *Kristallographiya* **1976**, *21*, 76.

in the range 3.21−3.26 Å).[24] Further evidence for this trend can be found in the structural features of the scheelite compounds $PbWO_4$ and $BiVO_4$. While $PbWO_4$ adopts the high-symmetry tetragonal structure at all temperatures studied, $BiVO_4$ undergoes a distortion to a monoclinic space group below 528 K.[16] This phase transition is driven by a small, but undeniable, lone pair distortion centered on the Bi^{3+} ion.

To better understand the bonding interactions that drive stereoactive lone pair distortions and the periodic trends that dictate crystal chemistry, we have carried out a computational study of the crystal chemistry of β-$SnWO_4$, $PbWO_4$, and both polymorphs of $BiVO_4$. The results reveal some interesting differences between Sn^{2+}, Pb^{2+}, and Sn^{2+}.

Experimental and Computational Methods

Synthesis. β-$SnWO_4$ was prepared from SnO and WO_3 using a conventional solid-state synthesis route. It was necessary to anneal in evacuated quartz tubes in order to prevent oxidation of tin to the tetravalent state. The β-$SnWO_4$ polymorph was obtained by heating at 780 °C,[25] whereas a 625 °C heat treatment produced the α-polymorph,[26] whose electronic structure will be described in greater detail in a subsequent publication.

Both polymorphs of $BiVO_4$ were obtained using a coprecipitation route in an aqueous solution followed by additional heat treatments. The zircon polymorph was prepared by adding 6.2 mmol of NH_4VO_3 to 5 mL of concentrated HNO_3. The mixture was then diluted to 50 mL with deionized water and heated under stirring until the red solid completely dissolved. In parallel, 6.2 mmol of $Bi(NO_3)_3 \cdot 5H_2O$ was added to 1 mL of concentrated HNO_3 and diluted to 10 mL with deionized water. The clear Bi^{3+} solution was then added to the red V^{5+} solution. The pH of this mixture was then increased by adding 7.5 mL of 3 M NH_4OH, causing the solution to become milky. Finally, an additional 25 mL of 3 M NH_4OH solution was added to complete the precipitation. The yellow precipitate must then be filtered without delay to prevent transformation to the fergusonite (distorted scheelite) polymorph. After drying, the product is a fine yellow powder with some transparent lustrous needle type crystals. Powder X-ray diffraction confirms the zircon structure of the product.[27] The fergusonite form of $BiVO_4$ was obtained by heating zircon $BiVO_4$ to 475 °C for 12 h.[28] The observation that the zircon form can be transformed to the fergusonite form by heating to a relatively low temperature or by allowing the precipitate to remain in contact with the solvent for an extended time strongly suggests that under ambient conditions fergusonite is the thermodynamically stable form of $BiVO_4$ and zircon is a metastable phase.

YVO_4 was prepared using a coprecipitation route similar to the one used to synthesize $BiVO_4$. In a 250 mL beaker, 14 mL of concentrated HCl, 0.5911 g of V_2O_5 and 1.3886 g of $Y_2(CO_3)_3 \cdot 3H_2O$ were mixed and heated at 80 °C. The hot solution was titrated with 3 M NH_4OH solution and 30% H_2O_2 until the pH reached ∼8 and the solution became a gel. The gel was filtered and dried to produce amorphous YVO_4. Polycrystalline YVO_4 was obtained heating at 350 °C for 3 h.[29] $PbWO_4$ was prepared from the reaction of PbO and WO_3 and at 1100 °C.

Diffuse Reflectance. The band gaps of the materials in this study were measured from polycrystalline samples using diffuse-reflectance spectroscopy.[30] Reflectance data were collected and converted to absorbance using a Perkin-Elmer Lambda 20 scanning double-beam spectrometer equipped with a 50 mm Labsphere integrating sphere over the spectral range 200−1100 nm (6.2−1.1 eV). The Kubelka−Munk function was used to convert the diffuse reflectance data into absorption data. Band gap energies quoted in this study are based on Shapiro's method of extrapolating the onset of absorption to the wavelength axis.[31]

Computational Methods. Geometry optimizations and density of states calculations were performed using the Cambridge Serial Total Energy (CASTEP) package.[32] CASTEP is a first principles density functional theory (DFT) plane wave pseudopotential simulation code. The calculations were performed in the frame of the generalized gradient approximation (GGA, Perdew−Wang 91) for the exchange and correlation effects.[33,34] Ultrasoft pseudopotentials corresponding to the optimization scheme of Vanderbilt were employed.[35] Calculations were performed with the accuracy of 0.1 eV/atom for total energy convergence.

Calculations were also carried out using version 47 of the Stuttgart tight bonding, linear muffin tin orbital, atomic sphere approximation (LMTO) code. LMTO is a self-consistent, DFT code, which incorporates scalar-relativistic corrections. Detailed descriptions of the ab initio calculations using the LMTO method are given elsewhere.[36,37] As was done with the CASTEP calculations, the effects of exchange and correlation were approximated using the Perdew−Wang generalized gradient approximation.

In order to gain a deeper insight to the nature of the lone pairs, the LMTO calculated electronic structures have been analyzed by means of the electron localization function (ELF)[38] and the cooperative orbital Hamiltonian overlap (COHP)[39] methods. The ELF is scaled to values between 0 and 1 with the meaning that the ELF values close to 1 correspond to highly localized electrons, as typically found for two-center two-electron bonds or nonbonding electron pairs in molecules.[40] COHP analysis is a partitioning scheme for the band structure energy (sum of the energies of the Kahn−Dham orbitals) in terms of orbital pair contributions. It provides a quantitative measure of bond strengths. All COHP curves presented here use positive values to represent bonding interactions and negative values for antibonding interactions.

Results and Discussion

Structural Description. In order to facilitate a discussion of the structure−property relationships, it is necessary to first review the crystal chemistry of AMO_4 compounds. The unit cells for the structure types of interest are shown in Figure 1. Scheelite (i.e., $BaWO_4$, $SrWO_4$, $CaWO_4$, ...) and zircon (i.e., $ZrSiO_4$, YVO_4, $DyVO_4$, $ErVO_4$, ...) are the symmetric structures that would be expected for the combination of a

(24) Nyburg, S. C.; Ozin, G. A.; Szymanski, J. T. *Acta Crystallogr. B* **1972**, *28*, 2885.
(25) Jeitschko, W.; Sleight, A. W. *Acta Crystallogr. B* **1974**, *30*, 2088.
(26) Jeitschko, W.; Sleight, A. W. *Acta Crystallogr. B* **1972**, *28*, 3174.
(27) Mariathasan, J.; Hazen, R.; Finger, L. *Phase Transitions* **1986**, *6*, 165.
(28) Liu, J.; Chen, J.; Li, D. *Acta Phys. Sin.* **1983**, *32*, 1053.
(29) Ropp, R.; Carroll, B. *Inorg. Nucl. Chem.* **1977**, *39*, 1303.
(30) Tandon, S. P.; Gupta, J. P. *Phys. Stat. Sol.* **1970**, *38*, 363.
(31) Shapiro, I. P. *Opt. Spektrosk.* **1958**, *4*, 256.
(32) Milman, V.; Winkler, B.; White, J. A.; Pickard, C. J.; Payne, M. C.; Akhmatskaya, E. V.; Nobes, R. H. *Int. J. Quant. Chem.* **2000**, *77*, 895.
(33) Perdew, J. P.; Chevary, J. A.; Vosko, S. H.; Jackson, K. A.; Pederson, M. R.; Singh, D. J.; Fiolhais, C. *Phys. Rev. B* **1992**, *46*, 6671.
(34) Perdew, J. P.; Wang, Y. *Phys. Rev. B* **1986**, 8600.
(35) Vanderbilt, D. *Phys. Rev. B* **1990**, *41*, 7892.
(36) Andersen, O. K. *Phys Rev. B* **1975**, *12*, 3060.
(37) Andersen, O. K.; Jepsen, O. *Phys. Rev. Lett.* **1984**, *53*, 2571.
(38) Becke, A. D.; Edgecombe, K. E. *J. Chem. Phys.* **1990**, *92*, 5397.
(39) Dronskowski, R.; Blöchl, P. E. *J. Phys. Chem.* **1993**, *97*, 8617.
(40) Fasser, T. F.; Savin, A. *Chem. Unserer Zeit.* **1997**, *31*, 110.

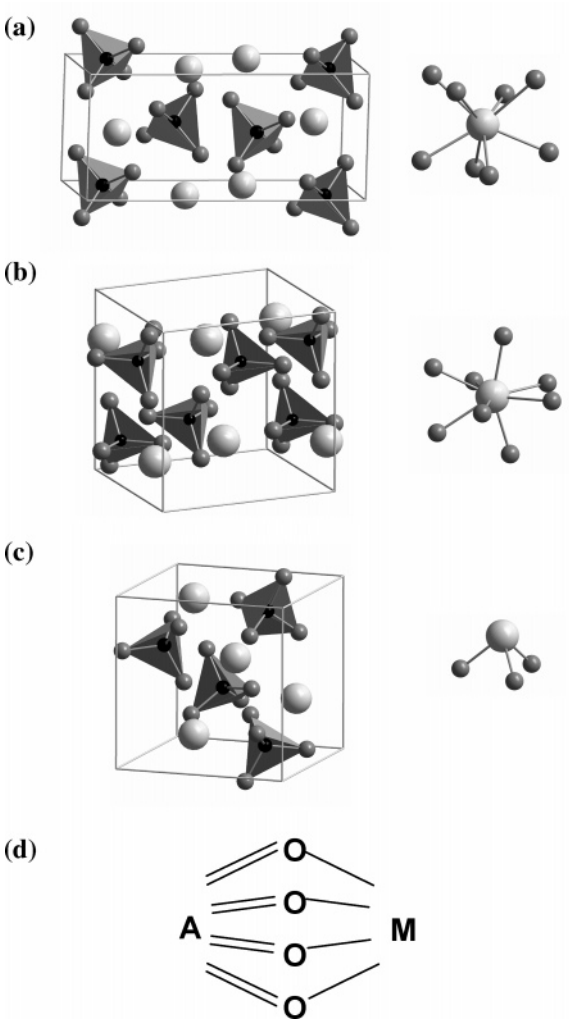

Figure 1. Structural depiction of the (a) scheelite $PbWO_4$, (b) zircon-$BiVO_4$, and (c) β-$SnWO_4$ structures, where the transition metal ions are represented as a black spheres, the oxygen ions as smaller dark gray spheres, and the p-block cations as larger light-gray spheres. The diagrams to the right show the coordination environment of the p-block cations, Pb^{2+}, Bi^{3+}, and Sn^{2+}, respectively. The bond graph of the symmetric scheelite and zircon structures is represented in part (d).

small cation preferring tetrahedral coordination and a larger cation capable of adopting eightfold coordination. Both structures obey Pauling's fifth rule (the rule of parsimony)[41] and Brown's rule of maximal symmetry,[42] as illustrated in the bond graph shown in Figure 1d. Both scheelite and zircon structures consist of isolated MO_4 tetrahedra connected by AO_8 antiprisms but differ in the way these polyhedra are connected. The symmetry of the large cation site in the scheelite is S_4, while in zircon it is D_{2d}. It is important to note that these site symmetries forbid the mixing of the s and p orbitals of the large cation that would normally be associated with a stereoactive lone pair distortion.

While $PbWO_4$ adopts the scheelite structure and the metastable form of $BiVO_4$ adopts the zircon structure, compounds containing ns^2 p-block cations typically favor more distorted structures. In some cases the symmetry reduction can be described as a distortion of a symmetric

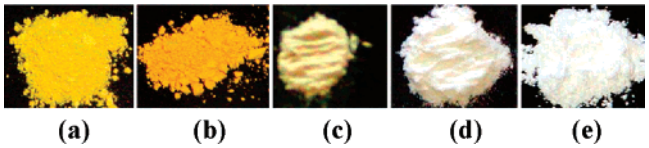

Figure 2. (a) zircon-$BiVO_4$, (b) fergusonite-$BiVO_4$, (c) β-$SnWO_4$, (d) $PbWO_4$, and (e) $BaWO_4$.

aristotype. This is the case for the thermodynamically stable form of $BiVO_4$, fergusonite. Fergusonite can be described as a monoclinic distortion of the scheelite structure. In fact, upon heating $BiVO_4$ transforms to the tetragonal scheelite structure at 528 K. Just above the phase transition (at 566 K) the BiO_8 antiprism has eight nearly equivalent distances (4×2.45 Å, 4×2.49 Å),[16] and the Bi^{3+} site symmetry is S_4. At room temperature in the monoclinic form the Bi^{3+} ion is shifted off center to produce a distorted environment with a wider range of Bi−O distances (2×2.35 Å, 2×2.37 Å, 2×2.52 Å, 2×2.63 Å),[43] and the Bi^{3+} site symmetry is lowered to C_2. It is important to note that mixing of the 6s and the 6p orbitals on bismuth is allowed for C_2 site symmetry but, as mentioned above, forbidden for the S_4 site symmetry of the scheelite form.

In other cases the lone pair distortion is so strong that the resulting crystal structure cannot be easily related to a structure where the p-block cation takes a symmetric coordination environment. The cubic structure of β-$SnWO_4$ (Figure 1c) represents such a case. This structure retains the WO_4^{2-} tetrahedral groups of the scheelite and zircon structures, but the coordination environment of the Sn^{2+} ion is best described as a three-coordinate trigonal pyramid. The C_3 site symmetry of the tin site allows mixing of the s and p_z orbitals, as would be required to satisfy Orgel's description of a stereoactive lone pair. The resulting Sn^{2+} coordination geometry is consistent with the ML_3E description of the central atom in the VSEPR scheme.

Diffuse Reflectance. Spectroscopic measurements provide an experimental tool for probing the electronic structure of a compound. Before turning to a discussion of the calculated electronic structures, let us consider the band gap excitation profiles of β-$SnWO_4$, $PbWO_4$, and $BiVO_4$ and compare their spectra with isostructural compounds where the ns^2np^0 cation has been replaced by an electropositive ns^0 cation. The ligand-to-metal charge transfer (LMCT) excitations of WO_4^{2-} and VO_4^{3-} groups fall in the ultraviolet region of the spectrum, at 6.2 and 4.5 eV, respectively.[44] These values are expected to be somewhat reduced in the ionic salts $BaWO_4$ and YVO_4 due to the formation of narrow bands. Nonetheless, the white coloration of $BaWO_4$ and YVO_4 (see Figure 2) shows that the LMCT excitations remain in the ultraviolet region of the spectrum. How do the optical properties change when Sn^{2+}, Pb^{2+}, or Bi^{3+} is introduced? Figure 2 shows that the zircon form of $BiVO_4$ is yellow, the

(41) Pauling, L. *J. Am. Chem. Soc* **1929**, *51*, 1010.
(42) Rao, G. H.; Brown, I. D. *Acta Crystallogr. B* **1998**, *54*, 221.
(43) Cox, D. E.; Moodenbaugh, A. R.; Sleight, A. W.; Chen, H. Y. *NBS Special Publication (U.S.)* **1980**, *567*, 189.
(44) Stuckl, A. C.; Daul, C. A.; Gudel, H. U. *J. Chem. Phys.* **1997**, *107*, 4606.
(45) Woodward, P. M.; Mizoguchi, H.; Kim, Y. I.; Stoltzfus, M. W. *Chemical Industries (Boca Raton, FL)* **2006**, *108*, (Metal Oxides), 133.

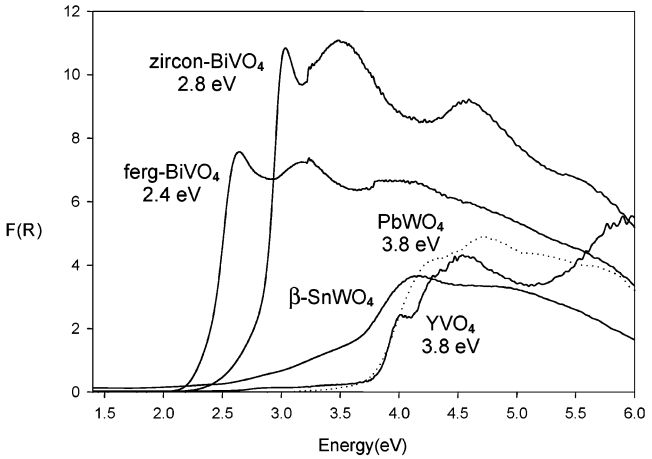

Figure 3. UV−visible diffuse reflectance spectra of fergusonite-$BiVO_4$, zircon-$BiVO_4$, β-$SnWO_4$, $PbWO_4$, and YVO_4.

fergusonite form of $BiVO_4$ is orange-yellow, β-$SnWO_4$ is a grayish-tan color, and $PbWO_4$ is an off-white color. The color change seen upon introduction of an ns^2 ion is a clear indication of a change in the electronic structure near the Fermi level.

For a more quantitative analysis consider the diffuse reflectance spectra shown in Figure 3. The band gap of YVO_4 ($E_g = 3.8$ eV) is reduced in the isostructural zircon type $BiVO_4$ ($E_g = 2.8$ eV), and the gap becomes even smaller in the fergusonite polymorph of $BiVO_4$ ($E_g = 2.4$ eV). The diffuse reflectance spectrum of $BaWO_4$ is not shown because the self-luminescence behavior of $BaWO_4$ complicates interpretation. However, the experimental band gap is reported to be 5.3 eV.[46] Once again we see that substitution of a ns^2 ion leads to a reduction in the band gaps of $PbWO_4$ ($E_g = 3.8$ eV) and β-$SnWO_4$ ($E_g \cong 2.6$ eV), although in the latter compound a rather broad transition makes it difficult to assign a precise value for band gap energy. The steepest part of the curve extrapolates to an energy of ~3.4 eV. In addition, there is clearly a lower-energy transition beginning at ~2.6 eV.

Geometry Optimization. The fist question to address computationally is the relative stability of the structural modifications that AMO_4 compounds can adopt. To do so, geometry optimizations were carried out using the CASTEP code for $PbWO_4$, $SnWO_4$, and $BiVO_4$ within the symmetry constraints of the scheelite, zircon, and β-$SnWO_4$ structure types. For $BiVO_4$ an additional optimization was carried out within the symmetry constraints of the monoclinic fergusonite structure (distorted scheelite). Key parameters of the geometry optimized structures are compared with the experimentally observed structures in Table 1.

The computed Pb−O, Sn−O, and Bi−O distances, as well as the unit cell dimensions, show excellent agreement with the experimentally observed parameters. The agreement is not quite as good for the W−O distances and the V−O distances of the zircon polymorph, where the computations yield bonds that are somewhat stronger and shorter than

(46) Kroger, F. A. *Some Aspects of the Luminescence of Solids;* Elsevier: New york, 1948.

Table 1. Selected Structural Parameters for the Experimental and Geometry-Optimized Calculated Structures[a]

compound	A−O distances (Å)	M−O distances (Å)	unit cell volume (Å^3)
	$PbWO_4$		
experimental	2.59(×4), 2.61(×4)	1.74(×4)	357.3
calculated	2.57(×4), 2.61(×4)	1.83(×4)	360.9
	$SnWO_4$		
experimental	2.21(×3), 2.81(×3)	1.75(×3), 1.76(×1)	388.9
calculated	2.21(×3), 2.79(×3)	1.83(×3), 1.82(×1)	388.8
	$BiVO_4$ (Zircon)		
experimental	2.41(×4), 2.55(×4)	1.70(×4)	351.2
calculated	2.39(×4), 2.52(×4)	1.74(×4)	351.8
	$BiVO_4$ (Fergusonite)		
experimental	2.35(×2), 2.37(×2), 2.52(×2), 2.63(×2)	1.69(×2), 1.77(×2)	309.2
calculated	2.36(×2), 2.38(×2) 2.51(×2), 2.64(×2)	1.68(×2), 1.77(×2)	310.2

[a] Geometry optimizations were performed with CASTEP code.

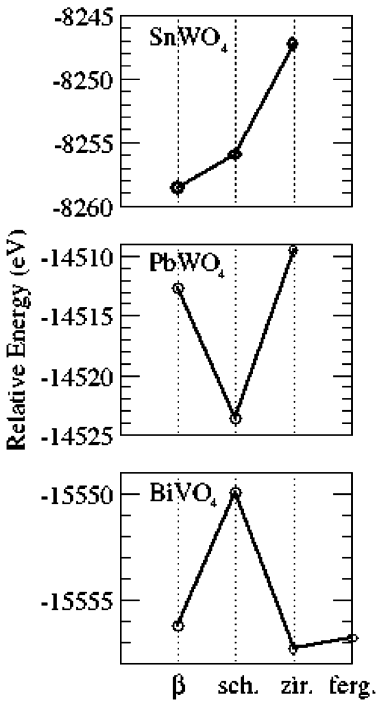

Figure 4. Relative energies as obtained from CASTEP geometry optimization calculations for $PbWO_4$ (squares), $SnWO_4$ (diamonds), and $BiVO_4$ (triangles). For $BiVO_4$ the fergusonite form is also shown.

observed. Nonetheless, the overall agreement between the computationally optimized structures and the observed structures is quite acceptable. This level of agreement is important to validate our comparisons between observed structures and hypothetical structures.

A comparison of the relative energies of the competing structure types for each composition is shown in Figure 4. In the case of $PbWO_4$ the total energy of the scheelite structure is seen to be 14.1 eV more stable than the hypothetical zircon form and 10.9 eV more stable than the hypothetical β-$SnWO_4$-type form. The computed total energy of the scheelite form of $PbWO_4$ is −14 523.6 eV, so that on a relative scale the scheelite structure has an energy that is 0.1% more stable than zircon and 0.08% more stable than β-$SnWO_4$-type structure. To put these differences in context,

it is relevant to note that neither of the hypothetical structures of $PbWO_4$ has been experimentally observed. Therefore, we will take these energy differences to be significant. The computations also correctly identify the observed β-$SnWO_4$ structure as having the lowest energy for $SnWO_4$. The total computed energy of β-$SnWO_4$ is -8258.6 eV, which is 2.6 eV (0.03%) lower in energy than the scheelite form and 11.3 eV (0.1%) more stable than the zircon form. The relatively small difference between the β-$SnWO_4$ and scheelite structures suggests it might be possible to prepare the scheelite polymorph under the proper conditions. The optimized unit cell volumes of 388.8 Å^3 for β-$SnWO_4$ and 365.7 Å^3 for scheelite suggests that high pressures might be effective in stabilizing the scheelite form of $SnWO_4$.

At first glance a comparison of the energies of the various structural modifications of $BiVO_4$ yields more ambiguous results. The most stable configuration is predicted to be the zircon form ($-15\,557.3$ eV), but the β-$SnWO_4$ type structure is competitive at an energy that is only 1.1 eV (0.007%) higher. The scheelite form is the least stable of the three (+7.4 eV, 0.05%), yet the experimental facts suggest that the monoclinic distortion of the scheelite structure, fergusonite, is the most stable modification. If the symmetry is lowered from the $I4_1/a$ space group symmetry of the scheelite structure to the $I112/b$ symmetry of the fergusonite structure, the energy of fergusonite ($-15\,556.8$ eV) becomes almost identical to that of zircon. Clearly, the various structural modifications are highly competitive with each other, consistent with the polymorphism observed for $BiVO_4$. However, it is important to note the stabilizing effect that the lone pair distortion of Bi^{3+} has on the scheelite structure.

Electronic Structures of WO_4^{2-} and $BaWO_4$. To better appreciate the role of the tin, lead, and bismuth cations in the electronic structures of the compounds under investigation, it is instructive to first consider the electronic structures of the polyatomic WO_4^{2-} and VO_4^{3-} ions. The molecular orbital diagram for a WO_4^{2-} group was calculated using the Amsterdam Density Functional package (results are shown in the supporting materials). The HOMO is a nonbonding linear combination of oxygen 2p orbitals with t_1 symmetry. The LUMO is the doubly degenerate set of W 5d−O 2p antibonding orbitals with e symmetry, while the next highest energy orbital is the triply degenerate t_2 set of similar orbital parentage. These latter two sets of molecular orbitals represent the well-known ligand field splitting of d orbitals in a tetrahedral environment. The lowest energy excitations for the tungstate group correspond to transitions from nonbonding oxygen 2p states to antibonding orbitals with significant tungsten 5d character, representing the classic case of LMCT. The magnitude of the HOMO−LUMO gap as calculated by ADF is 6.0 eV for WO_4^{2-} and 4.3 eV for VO_4^{3-}.[45] The experimental charge-transfer excitation energies for tungstate and vanadate groups are reported to be 6.2 and 4.5 eV, respectively.[44]

The electronic density of states (DOS) for $BaWO_4$ as calculated with CASTEP is shown in Figure 5. Rather than setting the Fermi level at zero energy, as is conventional practice, the energy scale in this diagram is referenced to the energy of the tungsten 4d core states in order to facilitate comparison with later calculations on $PbWO_4$ and $SnWO_4$. The valence band is split into two regions. The lower region (from -5.8 to -3.1 eV) has significant contributions from both W 5d and O 2p orbitals. In this region the W 5d−O 2p interaction is bonding, corresponding roughly to the W−O bonding 1e and $1t_2$ states in the WO_4^{2-} MO diagram. The upper region of the valence band (from -2.5 to 0.5 eV) is almost exclusively O 2p nonbonding in character and corresponds roughly to the t_1 and $2t_2$ molecular orbitals. The conduction band is also separated into two regions, both of which are W 5d−O 2p antibonding in character. The lower region (from 3.8 to 4.5 eV) and the upper region (from 6.0 to 7.5 eV) correspond roughly to the 2e and $3t_2$ MOs from the MO diagram of the tungstate group. The Ba 5s states are empty and make little contribution near the Fermi level. Inspection of the E vs k dispersion curves (not shown) shows a series of relatively flat bands. All of these features are consistent with the idea of $BaWO_4$ as an ionic salt with an electronic structure that originates directly from the electronic structure of the tungstate ion.

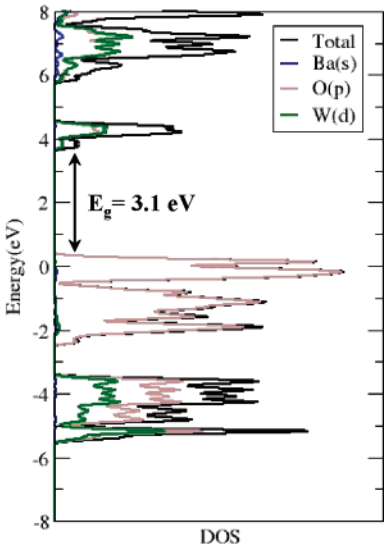

Figure 5. Total and partial density of states as obtained from CASTEP calculations for the scheelite form of $BaWO_4$. The energy scale in this diagram is referenced to the energy of the tungsten 4d core states (E_F = 0.25 eV).

The band structure calculations predict a band gap of 3.1 eV for $BaWO_4$, which is considerably smaller than the reported value of 5.3 eV.[46] The tendency for electronic band structure calculations to underestimate the band gap energy has been well documented in previous studies.[47−49] Despite this shortcoming, DFT calculations on oxides have proven effective in identifying key orbital interactions and reproducing trends.

Electronic Structures of $PbWO_4$ and $SnWO_4$. How does the electronic structure change when Ba^{2+} is substituted by either Sn^{2+} or Pb^{2+}? The electronic DOS plots for $PbWO_4$

(47) Eng, H. W.; Barnes, P. W.; Auer, B. M.; Woodward, P. M. *J. Solid State Chem.* **2003**, *175*, 94.
(48) Mizoguchi, H.; Eng, H. W.; Woodward, P. M. *Inorg. Chem.* **2004**, *43*, 1667.
(49) Mizoguchi, H.; Woodward, P. M. *Chem. Mat.* **2004**, *16*, 5233.

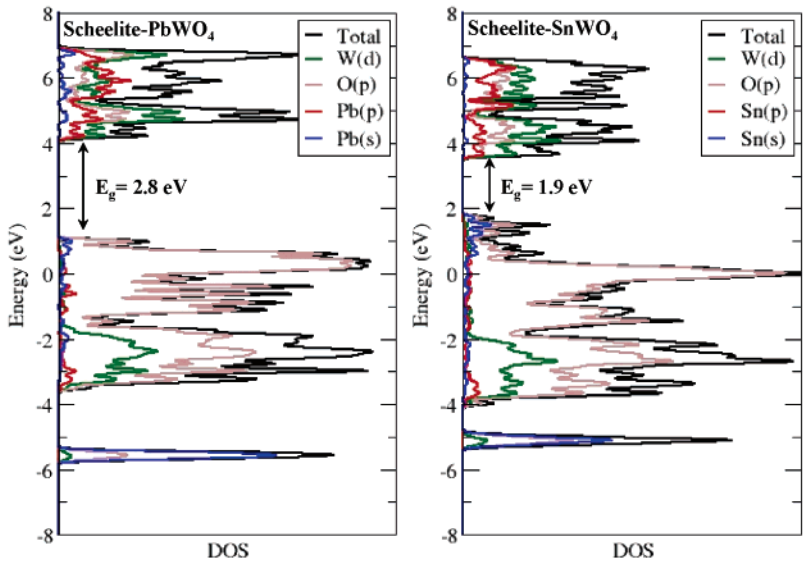

Figure 6. Total and partial density of states as obtained from CASTEP calculations for the scheelite form of $PbWO_4$ and $SnWO_4$. The energy scale in this diagram is referenced to the energy of the tungsten 4d core states (E_F = 1.0 eV for $PbWO_4$, E_F = 1.7 eV for $SnWO_4$).

and $SnWO_4$ in their geometry optimized scheelite forms are shown in Figure 6. With respect to the electronic structure of $BaWO_4$, it is possible to find both differences and similarities. Although the clean separation between the upper and lower parts of the valence band has been lost, there is still a clear transition from the bottom of the valence band where W 5d−O 2p bonding interactions dominate to the top of the valence band where O 2p nonbonding interactions are dominant. Unlike $BaWO_4$, there are now distinct states at the top and bottom of the valence band that originate from the presence of either the 6s orbitals of Pb or the 5s orbitals of Sn. In both $PbWO_4$ and $SnWO_4$ there is a very narrow band that is split off from the bottom of the O 2p valence band. The partial DOS plots show that the Pb 6s orbitals make the largest orbital contribution to this split-off band in $PbWO_4$, as do the Sn 5s orbitals in $SnWO_4$. However, there is a non-negligible amount of oxygen character also present, particularly in the case of $SnWO_4$. Thus, it would be more accurate to describe these states as *A ns*−O 2p bonding states rather than *A ns* nonbonding states. Of course, when there is a bonding interaction there must also be a corresponding antibonding interaction. In this case the *A ns*−O 2p antibonding interaction can be found at the top of the valence band. These antibonding interactions destabilize states at the top of the valence band and are largely responsible for the decrease in the band gap of $PbWO_4$ with respect to $BaWO_4$, as well as the larger decrease in the band gap of $SnWO_4$. The W 5d states enter the picture by mixing with the O 2p states, which will alter their interactions with valence orbitals on Sn (or Pb). Presumably, this plays a big role in the stabilization of a symmetric Pb^{2+} environment in $PbWO_4$ which contrasts sharply with the very distorted Pb^{2+} environment found in PbO.

The $PbWO_4$ partial density of states (PDOS) plot (Figure 6) reveals that the Pb 6s−O 2p bonding states that fall at roughly −6 eV have more Pb 6s character than O 2p character. The opposite description can be given for the Pb 6s−O 2p antibonding states that fall at roughly +1 eV. This indicates a two-level overlap scenario roughly equivalent to that depicted in Figure 7a. The relatively weak interaction

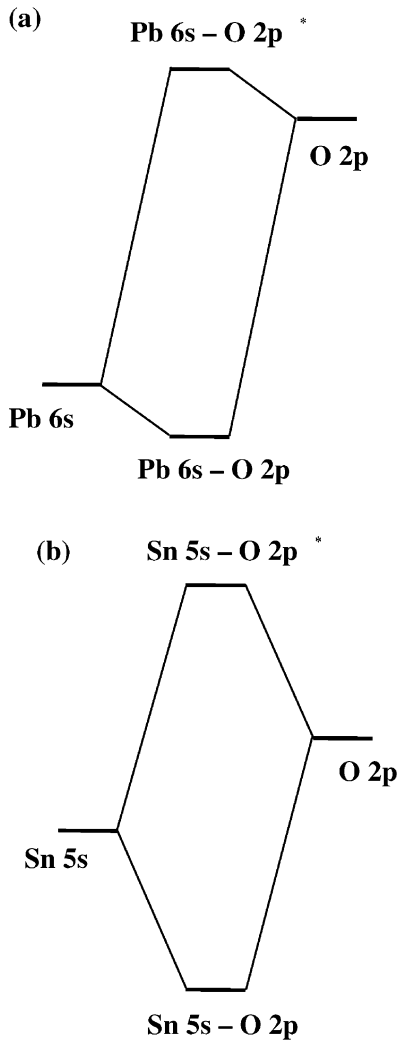

Figure 7. Schematic molecular orbital diagram showing (a) the interaction between the Pb 6s and O 2p orbitals and (b) the Sn 5s and O 2p orbitals.

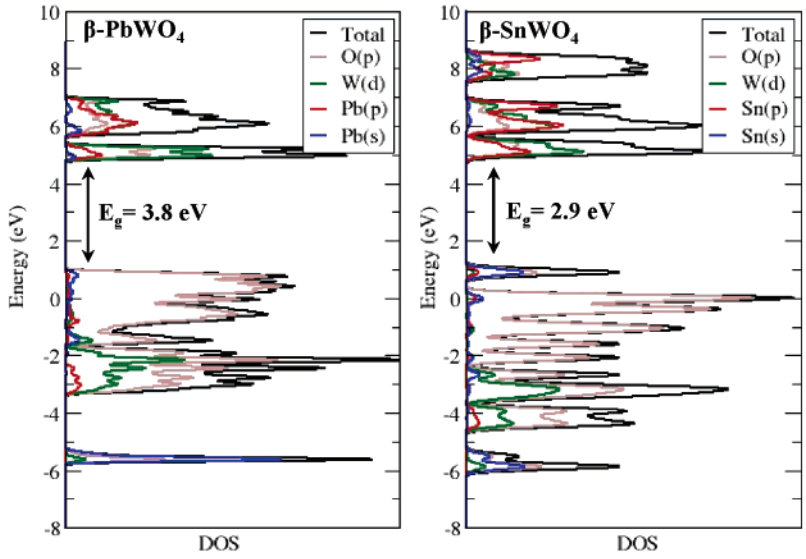

Figure 8. Total and partial density of states as obtained from CASTEP calculations for the β-$SnWO_4$-type structures of $PbWO_4$ and $SnWO_4$. The energy scale in this diagram is referenced to the energy of the tungsten 4d core states (E_F = 0.9 eV for $PbWO_4$, E_F = 1.0 eV for $SnWO_4$).

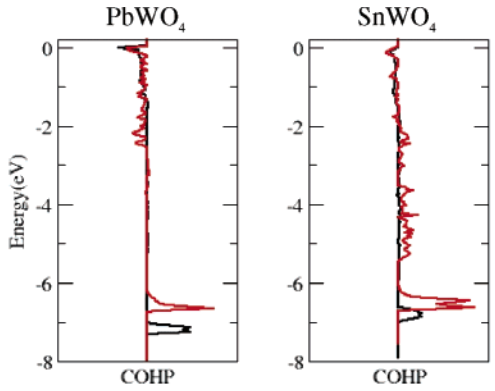

Figure 9. Cooperative overlap Hamiltonian population (COHP) plots calculated for the Pb 6s−O 2p interaction in $PbWO_4$ on the left and the Sn 5s−O 2p interaction in $SnWO_4$ on the right. The scheelite-type structure is shown in black, and the β-$SnWO_4$-type structure is shown in red. A positive COHP value indicates a bonding interaction, while a negative COHP indicates an antibonding interaction.

between the two orbitals explains the minor reduction in the band gap. In contrast, the PDOS plots for scheelite $SnWO_4$ show more equal participation of Sn 5s and O 2p orbitals in both the bonding and antibonding levels. Clearly, the Sn 5s−O 2p interaction is stronger than the Pb 6s−O 2p interaction, as represented schematically in Figure 7b. This leads to a more substantial destabilization of the O 2p states that make up the top of the valence band and a subsequently larger decrease in the band gap.

The differences in the electronic structures of these two compounds can be attributed to a relativistic contraction of the Pb 6s orbital, which diminishes the Pb 6s−O 2p interaction. This relativistic contraction is responsible for a fundamental difference in the bonding characteristics of the Pb^{2+} and Sn^{2+} ions. The Pb 6s−O 2p interaction is a weakly repulsive interaction between two sets of filled orbitals, whereas the Sn 5s−O 2p interaction is a strong repulsive interaction that gives rise to true bonding and antibonding levels, both of which are filled.

One of the basic concepts of molecular orbital theory is that interactions where both the bonding and antibonding levels are equally filled have a destabilizing influence. Hence, the symmetric scheelite forms of $PbWO_4$ and $SnWO_4$ are destabilized by the *A ns*−O 2p interactions, but the effect is much stronger in $SnWO_4$. The Sn 5s−O 2p antibonding interaction raises the energy of these states to the point where they are in close proximity to the unfilled states that make up the conduction band. In $SnWO_4$ the conduction band has not only W 5d−O 2p antibonding character, but also Sn 5p states. This raises the possibility for Sn 5s−O 2p−Sn 5p mixing. However, the site symmetry of tin in the scheelite structure prevents the Sn 5p states from mixing with the Sn 5s states. This sets up a situation that strongly favors a second-order Jahn−Teller (SOJT) distortion to a lower symmetry structure.[50,51] The symmetry of the distorted structure should be one that enables the Sn 5s and Sn 5p states to mix in order to stabilize the occupied Sn 5s−O 2p states near E_F, at the expense of empty states in the conduction band.

Figure 8 shows the electronic DOS for both $PbWO_4$ and $SnWO_4$ with the β-$SnWO_4$-type structure. First consider the electronic structure of β-$SnWO_4$ (Figure 8b). The C_3 site symmetry of the tin site in the β-$SnWO_4$ structure fully allows mixing of the Sn 5s and Sn $5p_z$ states, and such mixing is indeed observed. The increase of 1.0 eV in the band gap, with respect to the $SnWO_4$ with the symmetric scheelite structure, is very much consistent with a SOJT distortion. The Sn 5s−O 2p antibonding interactions found at the top of the valence band are clearly stabilized by introducing Sn 5p character. At the same time, the states split off at the top of the conduction band are Sn 5p−O 2p antibonding interactions that have been destabilized by introducing Sn 5s character. The band gap of $PbWO_4$ (Figure 8a) also increases by 1 eV upon changing from the scheelite-type to

(50) Halasyamani, P. S. *Chem. Mater.* **2004**, *16*, 3586.
(51) Halasyamani, P. S.; Poeppelmeier, K. R. *Chem. Mater.* **1998**, *10*, 2753.

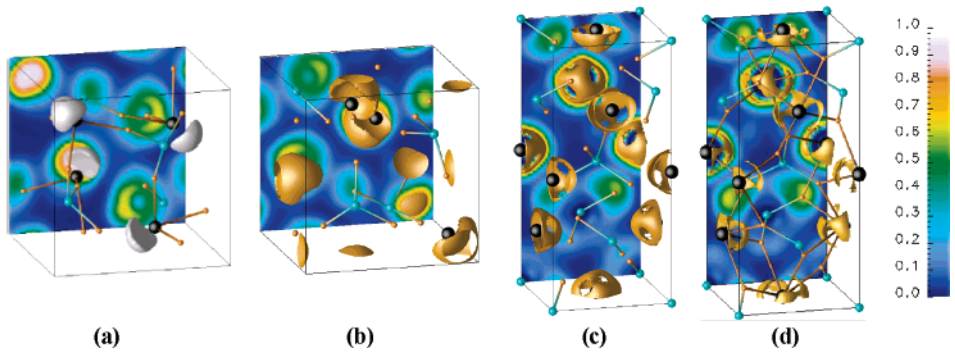

Figure 10. Electron localization functions as obtained from LMTO calculations for (a) β-$SnWO_4$, (b) $PbWO_4$ with the -$SnWO_4$ structure, (c) scheelite-$SnWO_4$, and (d) scheelite-$PbWO_4$.

the β-$SnWO_4$-type structure. However, the Pb 6s and 6p contributions at the top of the valence band are much smaller than the corresponding Sn 5s and 5p contributions in $SnWO_4$.

For a more quantitative comparison of the differences between Sn−O and Pb−O bonding, a COHP analysis was carried out. The Sn 5p−O 2p (Pb 6p−O 2p) bonding contribution across the valence band is much weaker than the corresponding Sn 5s−O 2p (Pb 6s−O 2p) contribution (see Supporting Information). Therefore, our discussion will be limited to the Sn 5s−O 2p (Pb 6s−O 2p) interaction. The Pb−O COHP plots across the valence band are shown for $PbWO_4$ in both structural modifications in Figure 9. A positive COHP value indicates a bonding interaction, while a negative COHP indicates an antibonding interaction. In the scheelite form we see bonding interactions at the bottom of the valence band and weaker antibonding interactions at the top of the valence band. This agrees with the description of bonding given above. Upon transforming to the β-$SnWO_4$-type structure, we see an increase in the antibonding Pb 6s−O 2p interactions at the top of the valence band but little increase in bonding interactions. This reduction in bonding can be quantified by integrating the area under the COHP curves. The integration yields a net bonding of 1.70 for the scheelite form vs 0.82 for the β-$SnWO_4$-type structure, confirming the increase in antibonding.

The COHP analysis of the Sn−O bonding across the valence band is shown on the right-hand side of Figure 9. The basic description of the bonding is not very different. However, now we see that transforming from the scheelite-type structure to the β-$SnWO_4$ structure leads to a marked increase in the Sn 5s−O 2p bonding. This occurs not only at the bottom of the valence band, but also throughout the lower half of the valence band. The net integrated area under the COHP curve goes from 2.00 in scheelite to 4.78 in β-$SnWO_4$. Thus, we see that transforming from a symmetric environment for Sn to one which exhibits a pronounced stereoactive lone pair distortion leads to a significant increase in the Sn 5s−O 2p bonding. It is interesting to observe that a similar effect is not observed for lead. This helps to explain the geometry optimization results.

To better visualize lone pairs associated with Sn^{2+} and Pb^{2+} cations, the ELFs are shown for scheelite and β-$SnWO_4$ forms of both $PbWO_4$ and $SnWO_4$ in Figure 10. As implied from the PDOS plots, a stereoactive lone pair of electron density can clearly be seen in the case of β-$SnWO_4$. Changing the structure to scheelite where mixing of the Sn 5s and Sn 5p orbitals is symmetry forbidden removes the stereoactive character of the lone pair and creates a region of localized electron density that is roughly spherical in shape. The ELF representation for $PbWO_4$ shows a similar dependence upon structure. However, even when $PbWO_4$ takes the β-$SnWO_4$-type structure, the degree of localization is reduced (as indicated by the color coding). Spatially the "lone pair" is more diffuse than it is in $SnWO_4$.

Electronic Structures of YVO_4 and $BiVO_4$. The electronic structure of YVO_4, which crystallizes with the zircon structure, is shown in Figure 11. There is a number of similarities with the electronic structure of $BaWO_4$. There is a transition from V 3d−O 2p bonding states in the lower half of the valence band to purely nonbonding O 2p states in the upper half of the valence band. The conduction band possesses antibonding V 3d−O 2p character. Similar to $BaWO_4$, the conduction bands are quite narrow, reflecting the large separation between VO_4^{3-} groups and the poor overlap of yttrium orbitals with the antibonding states of the vanadate groups. The separation between the lower-energy conduction band states, originating from the antibonding e states of the VO_4^{3-} tetrahedron, and the higher-energy conduction band states, originating from the antibonding t_2 states, is smaller in YVO_4 than in $BaWO_4$. This is a reflection of the smaller crystal field splitting expected for a 3d transition metal ion, which in turn comes from the reduced spatial extension of the V 3d orbitals (relative to the W 5d orbitals). The yttrium 4d states are empty and do not contribute significantly near the Fermi level. The experimental band gap for YVO_4 is 3.8 eV,[52,53] whereas the value calculated by CASTEP is 3.0 eV, which as with the other compounds underestimates the true value.

Just as the electronic structure of $PbWO_4$ can be considered a perturbation of the electronic structure of $BaWO_4$, the electronic structure of $BiVO_4$ can be described starting from the electronic structure of YVO_4. The electronic structures

(52) Jayaraman, A.; Kourouklis, G. A.; Espinosa, G. P.; Cooper, A. S.; Van, Uitert, L. G. *J. Phys. Chem. Solids* **1987**, *48*, 755.
(53) Duclos, S. J.; Jayaraman, A.; Espinosa, G. P.; Cooper, A. S.; Maines, R. G. *J. Phys. Chem. Solids* **1989**, *50*, 769.

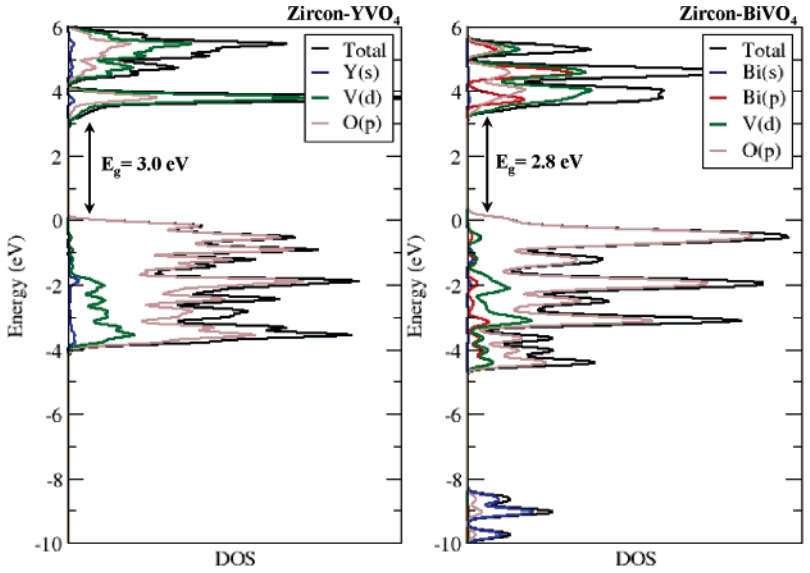

Figure 11. Total and partial density of states as obtained from CASTEP calculations for YVO_4 and $BiVO_4$ with the zircon structure. The energy scale in this diagram is referenced to the energy of the vanadium 3s core states ($E_F = 0.0$ eV for YVO_4, $E_F = 0.1$ eV for $BiVO_4$).

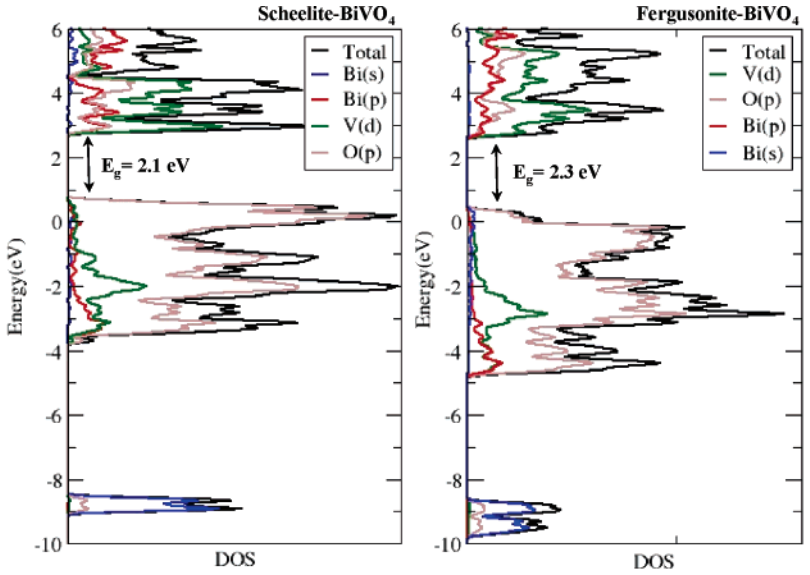

Figure 12. Total and partial density of states as obtained from CASTEP calculations for the scheelite and fergusonite form of $BiVO_4$. The energy scale in this diagram is referenced to the energy of the vanadium 3s core states ($E_F = 0.6$ eV for scheelite, $E_F = 0.7$ eV for fergusonite).

of these isostructural analogues are shown side by side for comparison in Figure 11. The basic features of the YVO_4 electronic structure are retained in $BiVO_4$, with the addition of a number of states that arise from the presence of the bismuth 6s and 6p orbitals. Upon moving from Pb^{2+} to Bi^{3+}, the increase in effective nuclear charge should lead to a further contraction and lowering of the energy of the 6s and 6p orbitals. The calculations confirm this expectation. The Bi 6s contribution is largely confined to the bands that appear between -8 and -10 eV. These states are stabilized with respect to the Pb 6s$-$O 2p σ states seen in $PbWO_4$ by roughly 3 eV. Furthermore, the PDOS plots show that the O 2p contribution to these nominally Bi 6s$-$O 2p bonding states, is diminished with respect to $PbWO_4$ (see Figures 6 and 8) The Bi 6p orbitals make a significant contribution to the conduction band, but interestingly, the energy of the conduction band does not change very much with respect to YVO_4. We also note that experimentally zircon $BiVO_4$ has a band gap (2.8 eV) that is roughly 1.0 eV smaller than YVO_4 (3.8 eV), whereas the computations predict only a small change in band gap upon moving from YVO_4 (3.0 eV) to $BiVO_4$ (2.8 eV).

Consider the electronic structure of $BiVO_4$ with the scheelite structure, as shown in Figure 12. It is instructive to compare it with scheelite $PbWO_4$ (Figure 6). As discussed in the previous paragraph, the Bi 6s states are energetically stabilized and their interaction with the O 2p orbitals is reduced, with respect to the Pb 6s states. As a result, the orbital character at the top of the valence band is almost completely oxygen 2p nonbonding. Interestingly, the calculated band gap is reduced from 2.8 eV in the zircon form to 2.1 eV in the scheelite form. As the lone pair is stereochemi-

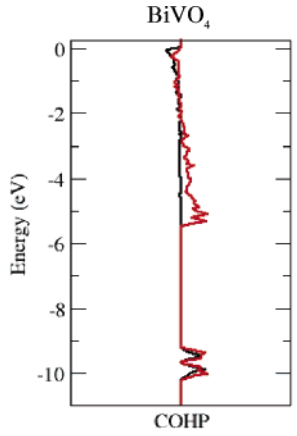

Figure 13. COHP plots calculated for the Bi 6s−O 2p interaction in $BiVO_4$, with the scheelite (shown in black) and fergusonite (shown in red) structures. A positive COHP value indicates a bonding interaction, while a negative COHP indicates an antibonding interaction.

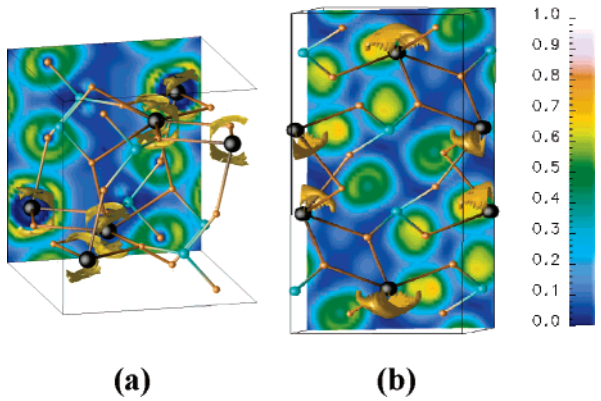

Figure 14. Electron localization functions as obtained from LMTO calculations for (a) zircon-$BiVO_4$ and (b) fergusonite-$BiVO_4$.

cally inactive in both scheelite and zircon, we see that the changes in color and band gap observed in Figures 2 and 3 are associated with the change in structure type/topology rather than from changes in the stereochemical activity of the Bi^{3+} ion.

The impact of the lone pair distortion can be directly assessed by comparing the electronic structures of $BiVO_4$ with the tetragonal scheelite structure and the monoclinic fergusonite structure, which are shown side by side in Figure 12. As expected, the SOJT distortion leads to an increase in the band gap, although the increase (2.1 to 2.3 eV) is rather modest. There is a noticeable stabilization that can be observed at the bottom of the O 2p valence band, which now extends downward by roughly an additional 1 eV. We can also see a small downward shift in the center of gravity of the Bi 6s states located at roughly 9 eV. However, unlike $SnWO_4$, the changes near the Fermi level are minor. This explains why the distortion has a rather small effect on the band gap.

Once again, we turn to a COHP analysis to examine the impact of the lone pair distortion on the *A ns*−O 2p bonding. The COHP analysis of the Bi−O bonding across the valence band is shown in Figure 13. Looking first at the scheelite form, with a symmetric Bi^{3+} environment, we see bonding interactions in the region dominated by Bi 6s states (−9 to −10 eV) and weaker antibonding interactions at the top of the O 2p valence band. This description is the same as we saw earlier for the scheelite forms of $PbWO_4$ and $SnWO_4$. The COHP for the zircon form (see Supporting Information) is very similar. Thus, this description seems generally applicable for structures with symmetric *A* cation site symmetries. Upon transforming to fergusonite, where the Bi^{3+} environment is distorted, we see an increase in the Bi 6s−O 2p bonding across the bottom half of the O 2p valence band, much like what was observed for $SnWO_4$ in Figure 9. The net integrated area under the COHP curve goes from 1.96 in scheelite to 2.25 in fergusonite. While it is true that the overall increase in bonding upon distorting the *A* cation environment is smaller for $BiVO_4$ than it is for $SnWO_4$, we should bear in mind that the lone pair distortion is also much smaller in the former case. What is most interesting is that Bi^{3+} behaves more like Sn^{2+} than Pb^{2+}.

A visual representation of the difference in the lone pair character can be seen in the ELF plots for zircon and fergusonite $BiVO_4$ shown in Figure 14. The zircon form has a symmetric region of electron localization, as expected from the site symmetry of the Bi^{3+} site. The more interesting comparison is between fergusonite $BiVO_4$ and β-$SnWO_4$. The "lone pair" in fergusonite has a smaller localization coefficient and its shape is noticeably different. The regions of localized electron density in the β-$SnWO_4$ ELF are very similar to the molecular orbital picture of a nonbonding electron lone pair, whereas the localized electron density in fergusonite $BiVO_4$ is more diffuse.

Conclusions

In ternary oxides containing Sn^{2+}, Pb^{2+}, and Bi^{3+} we see considerable differences in the orbital interactions responsible for stereoactive lone pair distortions. In $SnWO_4$ the Sn 5s orbitals interact strongly with O 2p orbitals. As both sets of orbitals are filled, this interaction destabilizes the oxygen 2p states at the top of the valence band, which would otherwise be nonbonding. This overlap creates an unstable bonding situation that is relieved by mixing with vacant Sn 5p−O 2p states in the conduction band via a SOJT distortion. The rehybridization that occurs produces a largely nonbonding lobe of localized electron density of Sn 5s−O 2p−Sn 5p orbital parentage that is strongly stereochemically active. The COHP analysis shows that the lone pair distortion leads to a significant increase in the Sn 5s−O 2p bonding interaction.

Upon replacing Sn^{2+} with Pb^{2+}, the valence shell s orbitals of the Group 14 cation undergo a relativistic contraction that reduces their interaction with the surrounding O 2p orbitals. This reduces the strength of the antibonding Pb 6s−O 2p interaction, which is the major driving force behind the SOJT distortion. As a consequence, the symmetric scheelite structure is stabilized. The COHP analysis shows that the preference for the scheelite structure originates in part from the fact that the distortion of Pb^{2+} environment does not result in an increase in the Pb 6s−O 2p bonding interaction.

Nevertheless, the Pb 6s orbitals are not completely inert; their presence does lead to a small decrease in the band gap.

The Bi^{3+} contribution to the electronic structure of $BiVO_4$ is in many ways similar to the Pb^{2+} contribution to the electronic structure of $PbWO_4$. However, the increased effective nuclear charge leads to a further stabilization of the 6s orbitals, diminishing the 6s contributions at the top of the valence band. Despite this stabilization, the driving force for a stereoactive lone pair distortion appears to be enhanced. The energies of structures exhibiting distorted Bi^{3+} environments are competitive with structures that possess symmetric Bi^{3+} environments. Comparison of the symmetric scheelite-type structure and the structurally related but distorted fergusonite structure is illustrative. The introduction of a lone pair distortion stabilizes the structure through increased Bi 6s−O 2p bonding. This behavior is reminiscent of Sn^{2+} in $SnWO_4$. However, the "lone pair" that is formed as a result of this distortion is not as localized as the Sn^{2+} lone pair in β-$SnWO_4$. Furthermore, the distortion has a much smaller impact on the electronic structure near the Fermi level.

Acknowledgment. The authors acknowledge funding from the National Science Foundation through their support of the Center for the Design of Materials (CHE-043567).

Supporting Information Available: Additional spectra and tables of crystallographic parameters. This material is available free of charge via the Internet at http://pubs.acs.org.

IC061157G